Research Article

A. A. Prikhodko*

Force analysis of the two-satellite planetary mechanism with elliptical gears

https://doi.org/10.2478/mme-2021-0006
Received Dec 12, 2020; accepted Mar 29, 2021

Abstract: Non-circular gears can be used in modern machines and mechanisms for the implementation of various types of motion and have high strength and compactness compared to linkage mechanisms. This article presents the force analysis of non-circular gear on the example of the planetary mechanism with elliptical gears, providing the rotationally reciprocating motion of the impeller of the stirred tank. Based on the calculation schemes of the links, kinetostatic balance equations for each link of the mechanism are compiled and solved. Reaction forces in kinematic pairs and balancing moment on the input shaft of the mechanism are found. The results can be used in the synthesis and analysis of various machines with the proposed kinematic scheme of the mechanism.

Keywords: Planetary gear, elliptical gears, rotationally reciprocating motion, kinetostatic analysis

1 Introduction

Transmissions by non-circular gears have been known for a long time and are of great interest to scientists and engineers [1, 2]. The first schemes of mechanisms with non-circular wheels were found in the works of Leonardo da Vinci, and some of the first models of such devices were made in the 19th century by the German scientist Ferdinand Redtenbacher. Widespread research and dissemination of these gears has long been hindered by the lack of simple and accurate manufacturing methods for non-circular gears.

Currently, there are a large number of papers devoted to geometric and kinematic analysis, design and practical application of gears by non-circular gears [3–9]. For example, there are proposed: chain drives with variable ratio for bicycles [3]; a mechanical device containing a Maltese cross mechanism and a gearing to achieve intermittent motion [4]; the gear trains used for velocity variation and function generation [5]; constructions of non-circular gears as a part of rotor hydraulic machines [6] and high-performance pumps [7]; a knee motion assist device for biomechatronic exoskeleton having grooved cams and non-circular wheels [8]; single planetary non-circular gears with one internal and one external gear for bicycles with high efficiency [9]. It was shown in [10–14] that planetary gears with non-circular wheels allow to change the sign of the transfer function and, therefore, provide different types of motion, for example, intermittent motion [10–12] or rotationally reciprocating motion [13, 14]. The proposed mechanisms are more compact and durable compared to linkages, and the improvement of high-precision equipment for machining and additive production stimulates the development of this issue of the mechanism and machine theory.

Non-circular gears can have various shapes, but elliptical gears are the most researched and widespread at the moment [15–17]. A large number of mechanisms and devices based on elliptical gears have been developed, their geometry and kinematics have been investigated [18–20], and various problems of their manufacture have been solved [21–23].

However, most of the papers on the creation of non-circular gears are devoted only to the geometry and kinematics of these mechanisms, while the issues of their dynamics are much more complex and have not been studied. Nevertheless, some applied problems of the dynamics of non-circular gears have been solved. For example, Xing Liu *et al.* [24] carried out a theoretical and experimental study of the dynamic performance of elliptical gears with rotational axes at the focus and center of the pitch ellipse. Nan Gao *et al.* [17] investigated parametric vibrations and instabilities of elliptical gears caused by loading torque and eccentricity vibrations. Zhiqin Cai and Chao Lin [25] presented and investigated a generalized nonlinear dynamic model of a curved gear drive based on Lagrange-Bondon graphs. Many researchers consider the issues of dynamics in relation to practical applications of mechanical devices [24–26] containing non-circular gears, since dynamic models include

***Corresponding Author: A. A. Prikhodko:** Department of Land Transport and Mechanics, Kuban State Technological University, 350072 Krasnodar, Russia; Email: sannic92@gmail.com

the parameters of technological load on the working body of the machine.

The purpose of this article is the kinetostatic analysis of a planetary mechanism with two external gears operating as part of a drive of a rotationally reciprocating stirred tank. The idea of imparting various non-stationary types of motion, including rotationally reciprocating motion, to the impeller of the stirred tank has been supported by many researchers around the world [27–29]. Despite the increasing complexity of the drive constructions, the prospects of this research area are due to a significant increase in the mixing efficiency, which has been experimentally confirmed using various practical examples [30, 31].

2 Formulation of the problem

The object of this research is the actuator of the stirred tank (Figure 1a), in which the rotational motion of the motor shaft is converted into the reciprocating motion of the impeller due to a planetary mechanism with elliptical gears (Figure 1b).

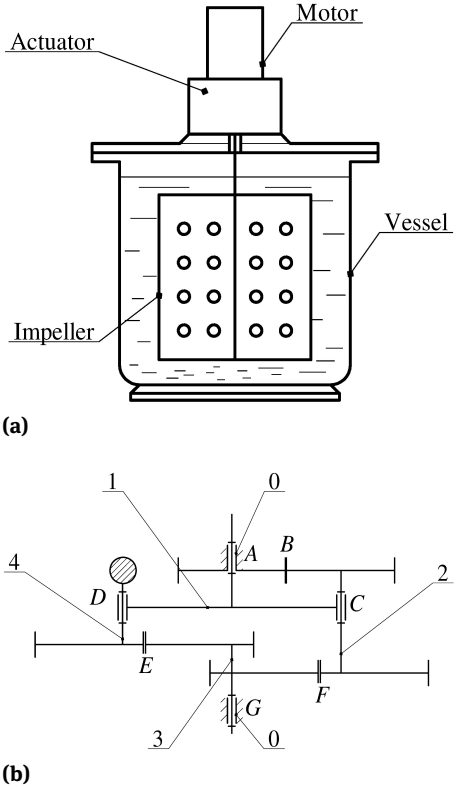

Figure 1: Rotationally reciprocating stirred tank: a – scheme of the actuator; b – structural scheme of the planetary mechanism

The proposed mechanism (Figure 1b) consists of rack 0, three-vertex links 1, 2, 3, two-vertex link 4, 1-DOF kinematic pairs A, C, D, G and 2-DOF kinematic pairs B, E, F. The structural analysis carried out in [13] showed that the mechanism exists in a three-moving space (translational displacements along the x and y axes and rotation around the z axis), which is traditionally called "planar." In the study of kinetostatics, we assume that all the kinematic pairs lie in the same plane. Figure 2 presents the calculation scheme of the mechanism. The angles of rotation of the input shaft together with the carrier and the output shaft are designated as φ_1 and φ_3, respectively.

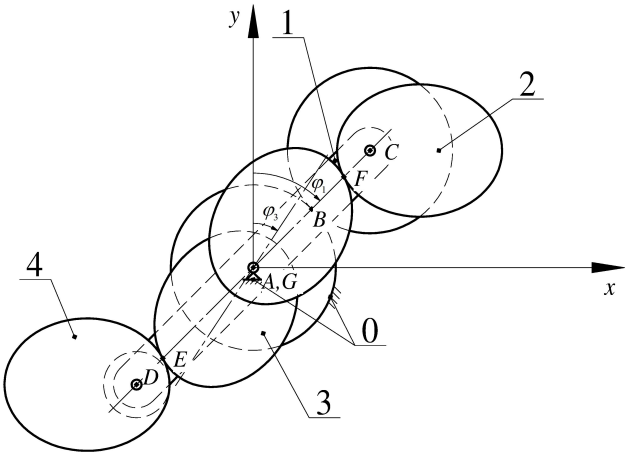

Figure 2: Calculation scheme of the mechanism

The study of kinetostatics was carried out for the actuator of the stirred tank, operating in the following mode: the frequency of the rotationally reciprocating motion f = 10 Hz, the swing angle of the impeller $\alpha = 150°$. For this mode, the following calculation data are considered known from [13, 14, 32]: active forces, moments of forces, masses and moments of inertia of links, as well as kinematic parameters (positions, velocities and accelerations). It is also assumed that the friction forces in the kinematic pairs are equal to zero.

3 Force analysis of the mechanism

Conducting a force analysis and determining reactions in kinematic pairs consists of writing and solving kinetostatic equations. In the proposed mechanism, for each link, it is necessary to compose 3 equations, in total 12 equations. The number of unknown reactions is also 12: 1 reaction in the kinematic pairs B, E, F and 2 components of the reaction

in the kinematic pairs A, C, D, G, and also the balancing moment M_b.

Force analysis is carried out sequentially for each link, beginnign with conducting a force analysis from link 4, since when it is released from bonds, the smallest number of unknown reactions is formed. In accordance with the d'Alembert principle, the acting forces and moments, as well as the forces and moments of force inertia were applied to link 4 (Figure 3).

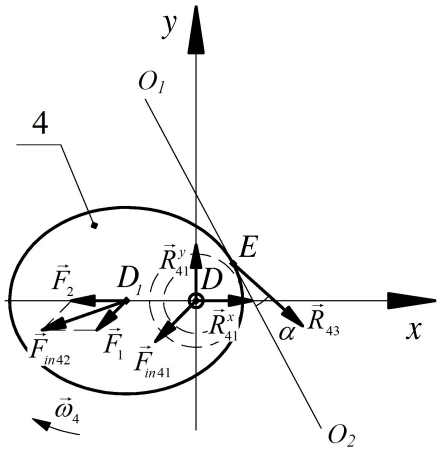

Figure 3: Calculation scheme of link 4

Link 4 makes plane-parallel motion, the instantaneous center of velocity, of which is the point on the sun wheel, opposite point B. Dynamic analysis showed [14, 32] that the angular velocity of the input link 1 is not a constant value due to the changes in the load on the impeller. However, when using the flywheel, the speed fluctuations are insignificant and do not have much effect on the forces acting on the links of the machine. Therefore, for the convenience of calculations, we assume that $\omega_1 = const$, $\omega_2 = const$ and $\omega_4 = const$.

Link 4 is affected by: a reaction $\vec{R}_{41}$ in kinematic pair D, the direction of which is not known in advance; reaction $\vec{R}_{43}$ in the kinematic pair E, which is directed at an angle α to the tangent O_1O_2; as well as inertial forces, which are applied to the center of mass of the link. Gravity forces are directed perpendicular to the plane of the figure, therefore, they are not projected on the x and y axes.

The lines O_1O_2, O_3O_4 (Figure 3(5)) make an angle γ with the axis Ox_2. Since O_3O_4 is a tangent to the ellipse at the point F, to determine the angle γ, the equation of the tangent in the plane Ox_2y_2 is written as [33, 34]:

$$\frac{x_0 \cdot x}{a^2} + \frac{y_0 \cdot y}{b^2} = 1 \tag{1}$$

where $x_0 = FG \cdot \sin(\varphi_1 - \varphi_3)$, $y_0 = FG \cdot \cos(\varphi_1 - \varphi_3) - OG$ are the coordinates of the point F in the plane Ox_2y_2, a and b are the semiaxes of the ellipse, $OG = c$ is the focal distance of the ellipse.

Transforming equation (1), we obtain an expression for finding γ:

$$\gamma = \operatorname{arctg}\left(-\frac{x_0}{y_0} \cdot \frac{b^2}{a^2}\right).$$

To determine the inertia forces, link 4 is considered as the sum of two bodies: body 4.1 (counterweight and satellite shaft), whose inertia force $\vec{F}_{in41}$ is applied to point D, and body 4.2 (elliptical wheel), whose inertia force $\vec{F}_{in42}$ is applied to point D_1.

The accelerations of points D and D_1 are defined as follows. Since $\varepsilon_1 = 0$, then $a_D = a_D^n = \omega_1^2 \cdot AD$. Taking point D as a pole, we obtain $\vec{a}_{D_1} = \vec{a}_D + \vec{a}_{D_1D}$, where $a_{D_1D} = a_{D_1D}^n = \omega_2^2 \cdot D_1D$ is the acceleration of point D_1 relative to pole D.

The required forces of inertia $\vec{F}_{in41}$ and $\vec{F}_{in42}$ are determined as:

$$\vec{F}_{in41} = m_{41} \cdot \vec{a}_D,$$

$$\vec{F}_{in42} = m_{42} \cdot \vec{a}_{D_1} = m_{42} \cdot \vec{a}_D + m_{42} \cdot \vec{a}_{D_1D}.$$

The notations $\vec{F}_1 = m_{42} \cdot \vec{a}_D$, $\vec{F}_2 = m_{42} \cdot \vec{a}_{D_1D}$ is introduced (Figure 3) and the equilibrium condition is written in the form of a system of three equations – the sum of the projections of all the forces on the x and y axis, and the sum of the moments relative to the point D:

$$R_{41}^x - (F_{in41} + F_1) \cdot \sin\varphi_1 - F_2 \cdot \sin(2\varphi_1) + R_{43} \cdot \cos(\gamma + \alpha - \varphi_3) = 0; \tag{2}$$

$$R_{41}^y - (F_{in41} + F_1) \cdot \cos\varphi_1 - F_2 \cdot \cos(2\varphi_1) - R_{43} \cdot \sin(\gamma + \alpha - \varphi_3) = 0; \tag{3}$$

$$\begin{aligned} F_1 \sin\left(\frac{\pi}{2} - \varphi_1\right) \cdot DD_1 \cdot \cos\left(\frac{\pi}{2} - 2\varphi_1\right) \\ + F_1 \cos\left(\frac{\pi}{2} - \varphi_1\right) \cdot DD_1 \cdot \sin\left(\frac{\pi}{2} - 2\varphi_1\right) \\ - R_{43}^x \cdot DE \cdot \cos(\pi + \varphi_1) \\ - R_{43}^y \cdot DE \cdot \sin(\pi + \varphi_1) = 0. \end{aligned} \tag{4}$$

Considering that $R_{43}^x = R_{43} \cdot \cos(\gamma + \alpha - \varphi_3)$ and $R_{43}^y = R_{43} \cdot \sin(\gamma + \alpha - \varphi_3)$, from (4), the reaction R_{43} is determined. Then, from equations (2) and (3), we find the reactions R_{41}^x and R_{41}^y.

Figure 4 shows the kinetostatic equilibrium of link 3. The link makes a rotationally reciprocating motion and

is affected by: reaction $\vec{R}_{30}$ in the kinematic pair G, the direction of which is not known in advance; reactions $\vec{R}_{32}$ and $\vec{R}_{34}$ in kinematic pairs F and E directed at an angle α to the tangents O_3O_4 and O_1O_2; normal $\vec{F}^n_{in3}$ and tangential $\vec{F}^\tau_{in3}$ inertia forces applied to the centers of mass of elliptical gears; moment of resistance of the stirred liquid $\vec{M}_r$ and moment of inertia forces $\vec{M}_{in3}$.

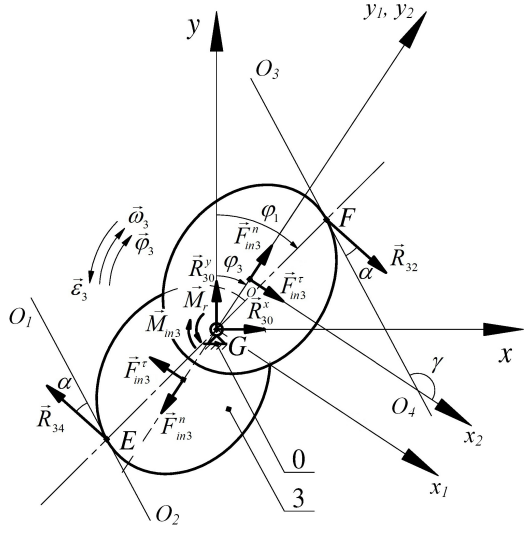

Figure 4: Calculation scheme of link 3

The kinetostatic balance condition is represented as a system of three equations – the sum of the projections of the all the forces on the x and y axis, and the sum of the moments relative to the point G:

$$R^x_{30} + R_{32} \cdot \cos(\gamma + \alpha - \varphi_3) - R_{34} \cdot \cos(\gamma + \alpha - \varphi_3) = 0; \quad (5)$$

$$R^y_{30} - R_{32} \cdot \sin(\gamma + \alpha - \varphi_3) + R_{34} \cdot \sin(\gamma + \alpha - \varphi_3) = 0; \quad (6)$$

$$M_r - M_{in3} - 2F^\tau_{in3} \cdot c - R^x_{32} \cdot FG \cdot \cos\varphi_1 - R^y_{32} \cdot FG \cdot \sin\varphi_1 - R^x_{34} \cdot EG \cdot \cos\varphi_1 - R^y_{34} \cdot EG \cdot \sin\varphi_1 = 0. \quad (7)$$

Considering that $R^x_{32} = R_{32} \cdot \cos(\gamma + \alpha - \varphi_3)$, $R^y_{32} = R_{32} \cdot \sin(\gamma + \alpha - \varphi_3)$, $R^x_{34} = R_{34} \cdot \cos(\gamma + \alpha - \varphi_3)$, $R^y_{34} = R_{34} \cdot \sin(\gamma + \alpha - \varphi_3)$, from equation (7), the reaction R_{32} is determined. Then, from equations (5) and (6), we find the reactions R^x_{30} and R^y_{30}.

Figure 5 presents the kinetostatic equilibrium of link 2, which performs the plane-parallel motion, the instantaneous center of velocity of which is point B. The link is affected by: a reaction $\vec{R}_{21}$ in kinematic pair C, the direction of which is not known in advance; reaction $\vec{R}_{23}$ in kinematic pair F, which is directed opposite to the found reaction $\vec{R}_{32}$; reaction $\vec{R}_{20}$ in kinematic pair B, which is directed at an angle α to the tangent O_5O_6; as well as inertia forces, which are applied to the center of mass of the link. For the convenience of solving the problem, as in the case of link 4, we consider link 2 as the sum of two bodies: body 2.1 (cylindrical wheel and satellite shaft), the inertia force $\vec{F}_{in21}$ of which is applied to point C, and body 2.2 (elliptical wheel), the inertia force $\vec{F}_{in22}$ of which is attached to the point C_1.

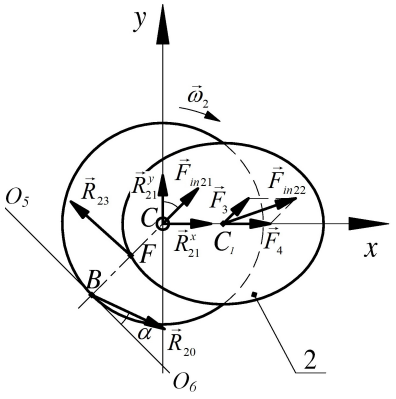

Figure 5: Calculation scheme of link 2

The accelerations of points C and C_1 are defined as follows. Since $\varepsilon_1 = 0$, then $a_C = a^n_C = \omega^2_1 \cdot AC$. Taking point C as a pole, we obtain $\vec{a}_{C1} = \vec{a}_C + \vec{a}_{C1}$, where $a_{C1} = a^n_{C1} = \omega^2_2 \cdot C_1$ is the acceleration of point C_1 relative to pole C.

The required forces of inertia $\vec{F}_{in21}$ and $\vec{F}_{in22}$ are determined as:

$$\vec{F}_{in21} = m_{21} \cdot \vec{a}_C,$$

$$\vec{F}_{in22} = m_{22} \cdot \vec{a}_{C1} = m_{22} \cdot \vec{a}_C + m_{22} \cdot \vec{a}_{C1}.$$

The notations $\vec{F}_3 = m_{22} \cdot \vec{a}_C$, $\vec{F}_4 = m_{22} \cdot \vec{a}_{C1}$ are introduced (Figure 5) and the equilibrium condition is written in the form of a system of three equations – the sum of the projections of all the forces on the x and y axis, and the sum of the moments relative to the point C:

$$R^x_{21} + (F_{in21} + F_3)\sin\varphi_1 + F_4 \sin(2\varphi_1) - R_{23}\cos(\gamma + \alpha - \varphi_3) + R_{20}\cos(\alpha - \varphi_1) = 0; \quad (8)$$

$$R^y_{21} + (F_{in21} + F_3)\cos\varphi_1 + F_4 \cos(2\varphi_1) + R_{23}\sin(\gamma + \alpha - \varphi_3) - R_{20}\sin(\alpha - \varphi_1) = 0; \quad (9)$$

$$F_3 \sin\left(\frac{\pi}{2} - \varphi_1\right) CC_1 \cos\left(\frac{\pi}{2} - 2\varphi_1\right) \quad (10)$$
$$+F_3 \cos\left(\frac{\pi}{2} - \varphi_1\right) CC_1 \sin\left(\frac{\pi}{2} - 2\varphi_1\right)$$
$$-R_{23}^x CF \cdot \cos(\pi + \varphi_1) - R_{23}^y CF \sin(\pi + \varphi_1)$$
$$+R_{20}^x BC \cos(\pi + \varphi_1) + R_{20}^y BC \sin(\pi + \varphi_1) = 0.$$

Considering that $R_{23}^x = R_{23} \cdot \cos(\gamma + \alpha - \varphi_3)$, $R_{23}^y = R_{23} \cdot \sin(\gamma + \alpha - \varphi_3)$, $R_{20}^x = R_{20} \cdot \cos(\alpha - \varphi_1)$, $R_{20}^y = R_{20} \cdot \sin(\alpha - \varphi_1)$, from (10), the reaction R_{20} is determined. Then, from equations (8) and (9), we find the reactions R_{21}^x and R_{21}^y.

Figure 6 shows the kinetostatic equilibrium of link 1, which performs a rotational motion. The link is affected by: a reaction $\vec{R}_{10}$ in kinematic pair A, the direction and module of which are unknown; a reaction $\vec{R}_{12}$ in kinematic pair C, which is directed opposite to the found reaction $\vec{R}_{21}$; reaction $\vec{R}_{14}$ in kinematic pair D, which is directed opposite to the found reaction $\vec{R}_{41}$; balancing moment $\vec{M}_b$.

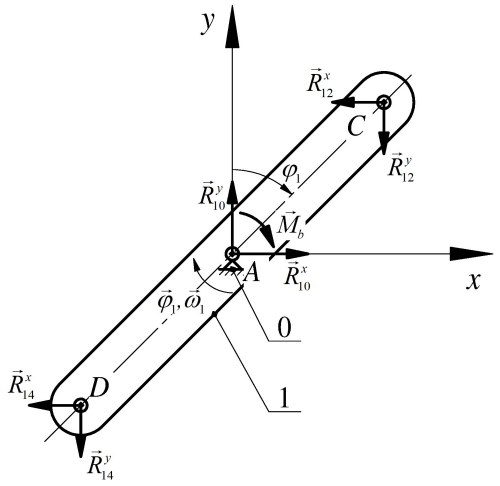

Figure 6: Calculation scheme of link 1

The kinetostatic balance condition is represented as a system of three equations – the sum of the projections of all the forces on the x and y axis, and the sum of the moments relative to the point A:

$$R_{10}^x - R_{12}^x - R_{14}^x = 0; \quad (11)$$

$$R_{10}^y - R_{12}^y - R_{14}^y = 0; \quad (12)$$

$$-M_y + R_{12}^x \cdot AC \cdot \cos\varphi_1 - R_{12}^y \cdot AC \cdot \sin\varphi_1 \quad (13)$$
$$-R_{14}^x \cdot AD \cdot \cos\varphi_1 + R_{14}^y \cdot AD \cdot \sin\varphi_1 = 0.$$

The unknown values $\vec{M}_b$, $\vec{R}_{10}^x$, $\vec{R}_{10}^y$ are found from equations (11) to (13).

4 Results

Mathematical modeling of kinetostatics is carried out for the rotationally reciprocating stirred tank with planetary actuator, developed on the basis of the Ika Magic Plant laboratory scale process plant (Figure 7). The developed experimental setup contains an electric motor 1, a motor control unit 2, a rack 3, on which the motor is fixed, a planetary actuator 4, an input shaft of an actuator 5, an output

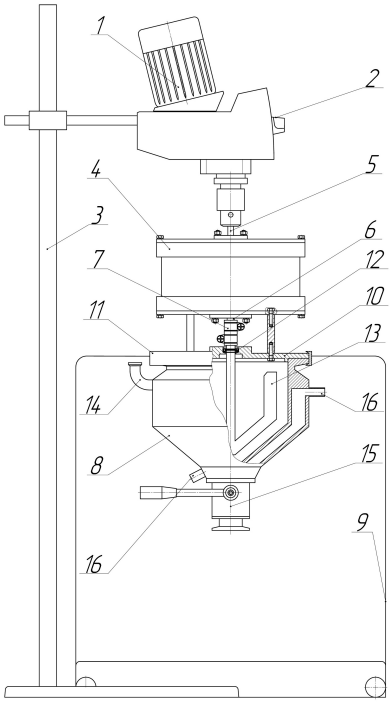

Figure 7: Ika Magic Plant laboratory scale process plant with rotationally reciprocating actuator

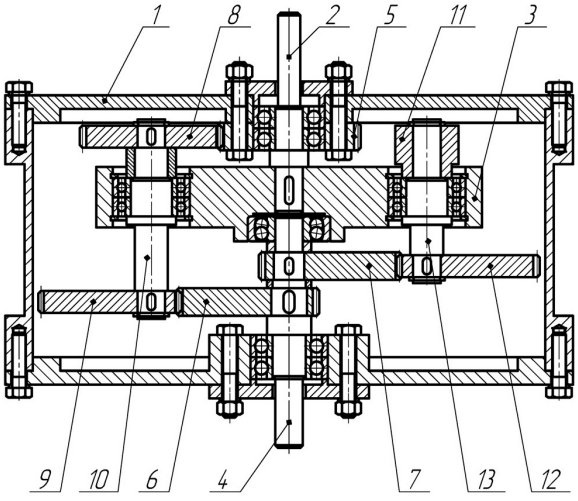

Figure 8: Design of planetary mechanism with elliptical gears

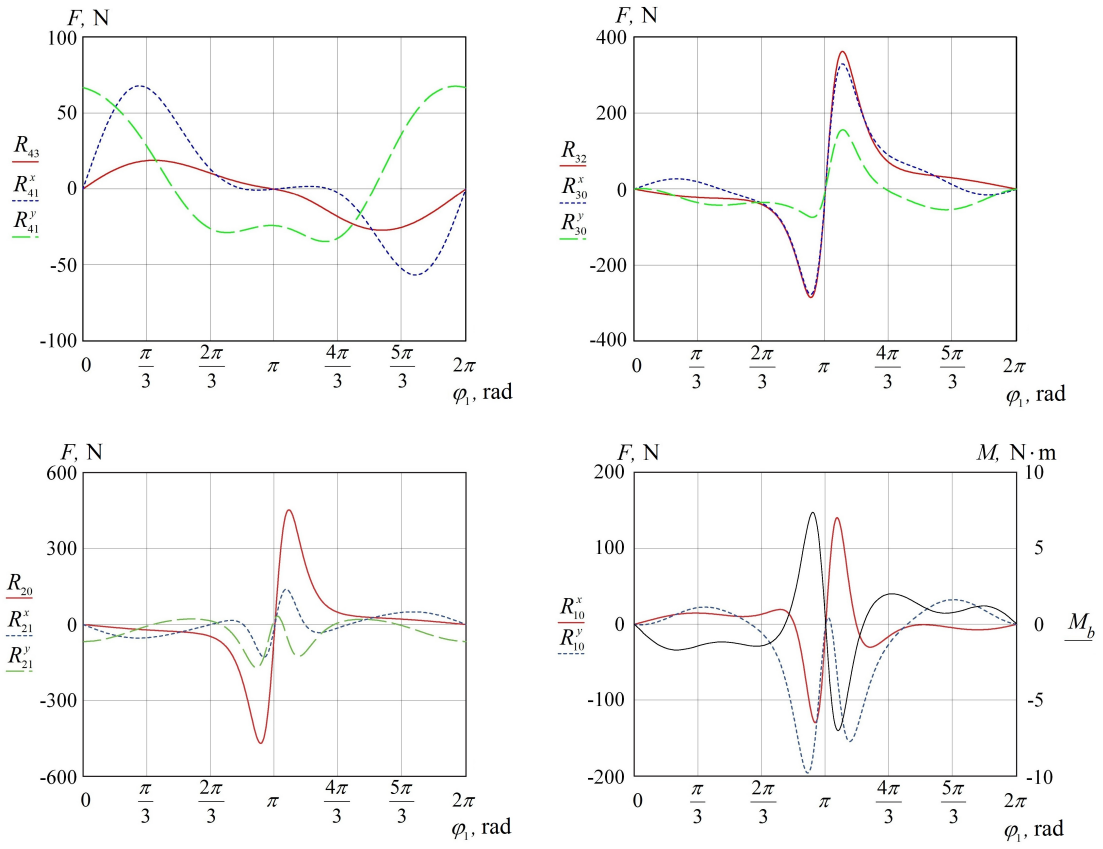

Figure 9: Graphs of reaction forces $R_i(\varphi_1)$ and balance moment $M_b(\varphi_1)$ in kinematic pairs

shaft of an actuator 6, a coupling 7, a reactor 8, a rack 9, which holds the reactor with the actuator, reactor cover 10, sealing clamp 11, impeller seal 12, impeller 13, product loading fitting 14, outlet valve 15, coolant supply fittings 16.

According to the structural scheme in Figure 1b, a planetary actuator is designed and manufactured (Figure 8). The design of the mechanism consists of the rack 1, an input shaft 2, a carrier 3, an output shaft 4, a sun wheel 5, elliptical gears 6 and 7 on the output shaft, located at an angle of 180°, a first satellite consisting of a cylindrical gear 8, an elliptical gear 9 and a shaft 10, a second satellite consisting of a counterweight 11, an elliptical wheel 12 and a shaft 13.

The links of the mechanism have the following inertial characteristics (the numbers of the links correspond to Figure 8): I_m = 100 g·cm^2 (motor); I_2 = 9.8 g·cm^2; I_3 = 1233 g·cm^2; I_4 = 30.4 g·cm^2; $I_6 = I_7$ = 627 g·cm^2; I_8 = 400 g·cm^2, m_8 = 0.1 kg; $I_9 = I_{12}$ = 564 g·cm^2, $m_9 = m_{12}$ = 0.09 kg; I_{10} = 19.2 g·cm^2, m_{10} = 0.04 kg; I_{11} = 350 g·cm^2, m_{11} = 0.09 kg; I_{13} = 25 g·cm^2, m_{13} = 0.05 kg; I_{im} = 15 g·cm^2 (impeller). By correlating the design of the mechanism (Figure 8) and the calculation schemes in Figures 3 to 6, we obtain the following masses and moments of inertia of the links for substitution in the kinetostatic equations (2) to (13): $I_1 = I_m + I_2 + I_3$ = 1342.8 g·cm^2; $I_3 = I_4 + I_6 + I_7 + I_{im}$ = 1299.4 g·cm^2; $m_{2.1} = m_8 + m_{10}$ = 0.14 kg; $m_{2.2} = m_9$ = 0.09 kg; $m_{4.1} = m_{11} + m_{13}$ = 0.14; $m_{4.2} = m_{12}$ = 0.09 kg.

A set of replaceable elliptical gears with eccentricities from 0.28 to 0.6 is manufactured for the planetary mechanism. Kinematic analysis of the mechanism is carried out in [14] by constructing plans of the link velocities for various eccentricities of elliptical gears, while the largest angle of rotation of the output shaft 147° is obtained at e = 0.6. The maximum angular speed of the motor shaft is 62.8 rad/s (n = 600 rpm), which allows to obtain the frequency up to 10 Hz of the rotationally reciprocating motion of impeller. Since the loads on the links of the mechanism increase with an increase in the frequency and angle of oscillation of the impeller, the kinetostatic analysis is carried out for the most loaded mode α = 150°, f = 10 Hz.

Studies of fluid dynamics in a reactor with a rotationally reciprocating motion of the impeller were carried out by various authors [35–37], equations for determining the Reynolds number and the moment of resistance on the working body were obtained. At the same time, researchers agree that in the case of laminar fluid motion, the moment

of resistance is proportional to the angular velocity of the impeller, and in turbulent motion, it is proportional to the square of the angular velocity. In the selected operating mode of the stirred tank, a turbulent mode of fluid movement is observed, therefore, according to [37], the following equation is applied to determine the moment of resistance M_r on the impeller:

$$M_r = B \cdot \omega_{im}^2 \cdot sign(\omega_{im}) \tag{14}$$

where B is the coefficient of resistance square law, ω_{im} is the angular velocity of the impeller. According to the results of calculations for the selected mode, $B = 2.67 \cdot 10^{-6}$ is obtained and used in further calculations.

After substituting the initial data and solving equations (2) to (13), the reactions in kinematic pairs is determined (Figure 9). Studies have shown that the most loaded are gears (kinematic pairs) B and F, and the rotational pair G.

Figure 9 presents graphs of the following reaction forces in kinematic pairs:

- functions of forces $R_{41}^x(\varphi_1)$, $R_{41}^y(\varphi_1)$ in kinematic pair D and force $R_{43}(\varphi_1)$ in kinematic pair E are shown in Figure 9a;
- functions of forces $R_{30}^x(\varphi_1)$, $R_{30}^y(\varphi_1)$ in kinematic pair G and force $R_{32}(\varphi_1)$ in kinematic pair F are shown in Figure 9b;
- functions of forces $R_{21}^x(\varphi_1)$, $R_{21}^y(\varphi_1)$ in kinematic pair C and force $R_{20}(\varphi_1)$ in kinematic pair B are shown in Figure 9c;
- functions of forces $R_{10}^x(\varphi_1)$, $R_{10}^y(\varphi_1)$ in kinematic pair A and balance moment $M_b(\varphi_1)$ are shown in Figure 9d.

As it can be seen from the graphs in Figure 9, the maximum values of the forces in the kinematic pairs and the balancing moment are observed during a change in the direction of rotation of the impeller (link 3). Moreover, in most cases, there is a change in the direction of the force and moment vector.

5 Conclusions

So, in this work, there are obtained systems of equations that allow to perform force analysis of the planetary actuator with elliptical gears and determine the reactions in kinematic pairs, as well as the balancing moment for all the positions of the mechanism. As an example, the calculations of the rotationally reciprocating stirred tank are carried out and the force graphs in kinematic pairs are presented, depending on the position of the mechanism, for the mode $f = 10$ Hz, $\alpha = 150^\circ$. The proposed methodology of force analysis can be implemented for other operating modes of the actuator, which allows for extensive studies of kinetostatics, to choose the most rational modes of operation of the stirred tank, as well as to simplify the calculation and design of the future machine. Also, the conducted studies can be applied in the design and analysis of other devices with the proposed scheme of the planetary mechanism.

Acknowledgement: The reported study was funded by RFBR according to the research project No. 18-31-00256.

References

[1] **Tarabarin V.B., Tarabarina Z.I.**: Model gears with variable ratios collected in Bauman Moscow State Technical University, *Proceedings of Higher Educational Institutions. Machine building*, 12, 84–91, **2014**.

[2] **Golovin A., Tarabarin V.**: *Russian Models from the Mechanisms Collection of Bauman University*, Springer Netherlands, Heidelberg, **2008**.

[3] **Freudenstein F., Chen C.K.**: Variable-ratio chain drives with noncircular sprockets and minimum slack-theory and application, *Journal of Mechanical Design*, 113(3), 253–262, **1991**.

[4] **Dooner D.B.**: Use of noncircular gears to reduce torque and speed fluctuations in rotating shafts, *Journal of Mechanical Design*, 119(2), 299–306, **1997**.

[5] **Litvin F.L., Gonzalez-Perez I., Fuentes A., Hayasaka K.**: Design and investigation of gear drives with non-circular gears applied for speed variation and generation of functions, *Computer Methods in Applied Mechanics and Engineering*, 197, 3783–3802, **2008**.

[6] **Efremenkov E.A., An I-Kan.**: Euler-Savari determination of radii of curvature of cycloid profiles, *Russian Engineering Research*, 30(10), 1001–1004, **2010**.

[7] **Liu D., Ba Y., Ren T.**: Flow fluctuation abatement of high-order elliptical gear pump by external noncircular gear drive, *Mechanism and Machine Theory*, 134, 338–348, **2019**.

[8] **Terada H., Zhu Y., Suzuki M., Cheng C., Takahashi R.**: Developments of a knee motion assist mechanism for wearable robot with a non-circular gear and grooved cams, *Mechanisms and Machine Science*, 3, 69–76, **2012**.

[9] **Mundo D.**: Geometric design of a planetary gear train with noncircular gears, *Mechanism and Machine Theory*, 41, 456–472, **2006**.

[10] **Zheng F., Hua L., Han X., Li B., Chen D.**: Linkage model and manufacturing process of shaping non-circular gears, *Mechanism and Machine Theory*, 96, 192–212, **2016**.

[11] **Zheng F., Hua L., Han X., Li B., Chen D.**: Synthesis of indexing mechanisms with non-circular gears, *Mechanism and Machine Theory*, 105, 108–128, **2016**.

[12] **Prikhodko A.A., Smelyagin A.I., Tsybin A.D.**: Kinematics of planetary mechanisms with intermittent motion, *Procedia Engineering*, 206, 380–385, **2017**.

[13] **Smelyagin A.I., Prikhod'ko A.A.**: Structure and kinematics of a planetary converter of the rotational motion into the reciprocating rotary motion, *Journal of Machinery Manufacture and Reliability*, 45(6), 500–505, **2016**.

[14] **Prikhodko A.A., Smelyagin A.I.**: Dynamics of rotationally reciprocating stirred tank with planetary actuator, *Journal of Physics: Conference Series*, 858, 012026, **2017**.

[15] **Danieli G.A., Mundo D.**: New developments in variable radius gears using constant pressure angle teeth, *Mechanism and Machine Theory*, 40, 203–217, **2005**.

[16] **Karpov O., Nosko P., Fil P., Nosko O., Olofsson U.**: Prevention of resonance oscillations in gear mechanisms using non-circular gears, *Mechanism and Machine Theory*, 114, 1–10, **2017**.

[17] **Gao N, Meesap C, Wang S, Zhang D.**: Parametric vibrations and instabilities of an elliptical gear pair, *Journal of Vibration and Control*, 26, 1721–1734, **2020**.

[18] **Liu J.Y., Chang S.L., Mundo D.**: Study on the use of a non-circular gear train for the generation of Figure-8 patterns, *Proceedings of the Institution of Mechanical Engineers, Part C: Journal of Mechanical Engineering Science*, 220, 1229–1236, **2006**.

[19] **Prikhodko A.A.**: Experimental kinematic analysis of an intermittent motion planetary mechanism with elliptical gears, *Journal of Measurements in Engineering*, 8, 122–131, **2020**.

[20] **Maláková S., Urbanský M., Fedorko G., Molnár V., Sivak S.**: Design of Geometrical Parameters and Kinematical Characteristics of a Non-Circular Gear Transmission for Given Parameters, *Applied Sciences*, 11, 1000, **2021**.

[21] **Chang S.L., Tsay C.B., Wu L.I.**: Mathematical model and undercutting analysis of elliptical gears generated by rack cutters, *Mechanism and Machine Theory*, 31, 879–890, **2006**.

[22] **Bair B.W.**: Computerized tooth profile generation of elliptical gears manufactured by shaper cutters, *Journal of Materials Processing Technology*, 122, 139–147, **2002**.

[23] **Figliolini G., Angeles J.**: The synthesis of elliptical gears generated by shaper-cutters, *Journal of Mechanical Design*, 125, 793–801, **2003**.

[24] **Liu X., Nagamura K., Ikejo K.**: Analysis of the dynamic characteristics of elliptical gears, *Journal of Advanced Mechanical Design, Systems, and Manufacturing*, 6, 484–497, **2012**.

[25] **Cai Z., Lin C.**: Dynamic model and analysis of nonlinear vibration characteristic of a curve-face gear drive, *Strojniski Vestnik-Journal of Mechanical Engineering*, 63, 161–171, **2017**.

[26] **Zhao Y., Yu G.H., Wu C.Y.**: Circuit Simulation and Dynamic Analysis of a Transplanting Mechanism with Planetary Elliptical Gears, *Transactions of the ASABE*, 54, 1179–1188, **2011**.

[27] **Senda S., Komoda Y., Hirata Y., Takeda H., Suzuki H., Hidema R.**: Fluid deformation induced by a rotationally reciprocating impeller, *Journal of Chemical Engineering of Japan*, 47, 151–158, **2014**.

[28] **Wójtowicz R.**: Flow pattern and power consumption in a vibromixer, *Chemical Engineering Science*, 172, 622–635, **2017**.

[29] **Torubarov N.N., Serov M.V., Malyshev R.M., Torubarov S.N.**: Design of actuator of the drives of nonstationary mixers, *Chemical and Petroleum Engineering*, 54, 552–559, **2018**.

[30] **Kato Y., Tada Y., Ban M., Nagatsu Y., Iwata S., Yanagimoto K.**: Improvement of mixing efficiencies of conventional impeller with unsteady speed in an impeller revolution, *Journal of chemical engineering of Japan*, 38(9), 688–691, **2005**.

[31] **Date T., Komoda Y., Suzuki H., Hidema R., Suzuki K.**: Application of a rotationally reciprocating plate impeller on crystallization process, *Journal of Chemical Engineering of Japan*, 51, 159–165, **2018**.

[32] **Prikhodko A.A.**: *Synthesis and analysis of the planetary actuator of the rotationally reciprocating stirred tank*, Ph. D. Thesis, Mechanical Engineering Research Institute RAS, **2019**.

[33] **Ilyin V.A., Poznyak E.G.**: *Analytical geometry*, Fizmatlit, Moscow, **2004**.

[34] **Coxeter H.S.M.**: *Introduction to Geometry*, Wiley, New York, **1969**.

[35] **Senda S., Yamagami N., Komoda Y., Hirata Y., Suzuki H., Hidema R.**: Power characteristics of a rotationally reciprocating impeller, *Journal of chemical engineering of Japan*, 48(11), 885–890, **2015**.

[36] **Woziwodzki S.**: Unsteady Mixing Characteristics in a Vessel with Forward-Reverse Rotating Impeller, Chemical Engineering & Technology, 34(5), 767–774, **2011**.

[37] **Prikhod'ko A.A., Smelyagin A.I.**: Investigation of power consumption in a mixing device with swinging movement of the actuating element, *Chemical and Petroleum Engineering*, 54 (3-4), 150≠155, **2018**.